Polarization spectroscopy of rubidium atoms: Theory and experiment

Huy Diep Do, Geol Moon, and Heung-Ryoul Noh*

Department of Physics and Institute of Opto-Electronic Science and Technology, Chonnam National University, Gwangju 500-757, Korea

(Received 13 October 2007; published 27 March 2008)

We present a theoretical and experimental study of polarization spectroscopy of rubidium atoms. All of the populations of the magnetic sublevels were calculated from the rate equations and used in the calculation of the polarization spectroscopy spectra. Using this model, we could generate theoretical line shapes of the polarization spectra on the D_2 transitions of rubidium atoms. The experimental results demonstrated that our model accurately reproduced spectra for all transitions in hyperfine structures.

DOI: 10.1103/PhysRevA.77.032513 PACS number(s): 32.30.−r, 42.62.Fi, 32.70.Jz

I. INTRODUCTION

Polarization spectroscopy (PS), first demonstrated by Wieman and Hänsch in 1976 [1], has drawn considerable attention from researchers in atomic, molecular, and chemical physics fields [2]. The most important applications of PS are laser frequency locking [3–8] and spectroscopic measurements in flames [9] and in plasmas [10]. In PS, the observed signal is the change in the polarization state of a weak and linearly polarized probe beam resulting from optical anisotropy induced by a strong circularly polarized counter propagating pump beam. Analogous to saturation spectroscopy [2,11,12], optical pumping plays an important role as a mechanism for producing anisotropy in PS.

From the perspective of experimental work, there have been many reports so far, mostly for laser frequency stabilization [3–8]. In contrast, there have been few reports on the accurate calculation of PS spectra. A theoretical model developed by Nakayama combining the theory of birefringence and dichroism with the first-order theory of velocity selective optical pumping has been widely used in estimating the PS spectra [13,14]. Although this model provides rather reasonable results, it still fails to provide an accurate theoretical calculation of the PS spectra. Recently, Harris *et al.* reported a theoretical study by solving rate equations [15]. Experimental results showed that the transitions from the upper hyperfine level of the ground state gave good agreement with theoretical predictions. However, this model was unable to accurately account for the results for the transitions from the lower hyperfine level of the ground state [15].

In this paper, we present a theoretical calculation of the PS spectra based on a rate equation model. We generated PS spectra by calculating the induced optical anisotropy for all the laser detunings. By using the developed model, we could account for the experimental results very accurately. This paper is organized as follows. In the next section, we explain the rate equation model utilized in calculating the PS spectra. In Sec. III, we describe experimental apparatus used to verify our model. The results and discussions follow in Sec. IV. We present conclusions in the final section.

II. THEORY

In this section, we present calculations for the PS spectra for D_2 line of the alkali-metal atom based on the assumption of rate equation approximation. The schematic of PS is shown in Fig. 1. A σ^+-polarized pump beam propagates along the $-z$ direction and a linearly polarized probe beam $(\hat{x}\cos\theta+\hat{y}\sin\theta)$ propagates along the z direction with $\theta \simeq \pi/4$. After traversing a rubidium cell with a length of L, the electric field becomes

$$\vec{E} = \frac{E_0}{\sqrt{2}}[-\hat{\epsilon}_+ e^{-\alpha_+ L/2} e^{i(kn_+ L-\theta)} e^{ikL(\mu_+ + i\nu_+)} + \hat{\epsilon}_- e^{-\alpha_- L/2} e^{i(kn_- L+\theta)} e^{ikL(\mu_- + i\nu_-)}], \quad (1)$$

where $n_\pm$ $(\alpha_\pm)$ is the refractive index (absorption coefficient) of the rubidium vapor and $\mu_\pm + i\nu_\pm$ is the complex refractive index by the windows for the $\sigma^\pm$ component of the probe beam $\hat{\epsilon}_\pm = \mp(\hat{x} \pm i\hat{y})/\sqrt{2}$ and k is the wave vector. In reality, $\mu_\pm$ and $\nu_\pm$ are much smaller than the refractive index of $n_\pm$ [2].

Since $\eta_+ \simeq \eta_-$ ($\eta = n, \alpha, \mu$, and ν), we define the quantities η (mean value) and $\Delta\eta$ (difference) as $\eta_\pm = \eta \pm \frac{\Delta\eta}{2}$. Then Eq. (1) becomes approximately linearly polarized with an inclination angle of $\theta - (kL/2)(\Delta n + \Delta\mu)$ made with the x axis. Finally the intensity difference $\Delta I = I_x - I_y$ is given by

$$\Delta I \cong I_0 \left[\frac{\pi}{2} - 2\theta + kL(\Delta n + \Delta\mu) \right], \quad (2)$$

where $I_0 = \frac{1}{2}\epsilon_0 c E_0^2 \exp[-(\alpha + 2k\nu)L]$ is the attenuated intensity of the incident probe laser beam. To measure the effect of the pump beam only (i.e., Δn), we set

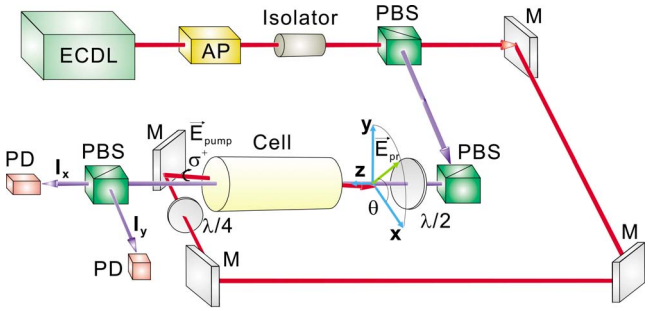

FIG. 1. (Color online) An experimental schematic of polarization spectroscopy: external cavity diode laser (ECDL); anamorphic prism pair (AP); quarter-wave plate (λ/4); half-wave plate (λ/2); polarizing beam splitter (PBS); mirror (M); and photodiode (PD).

*hrnoh@chonnam.ac.kr

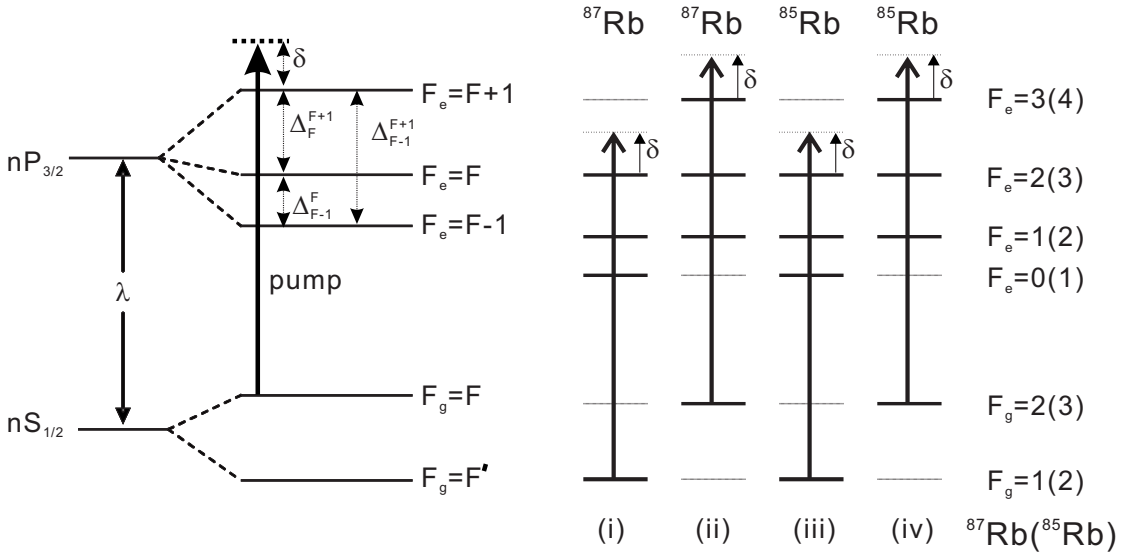

FIG. 2. An energy level diagram of the D_2 transition of an alkali-metal atom: Four experimental schemes [(i), (ii), (iii), and (iv)] for ^{87}Rb and ^{85}Rb atoms are presented.

$\theta=\pi/4+(kL/2)\Delta\mu$, and Eq. (2) becomes the following equation:

$$\Delta I = I_0 kL\Delta n. \tag{3}$$

The other phenomena which might affect the polarization of the probe beam such as the polarizing beam splitters can also be included in Eq. (2), and can be compensated by adjusting the value of θ. In Eq. (3), we can see that the polarization spectra observed in the experiment are proportional to the refractive index difference Δn.

Now we calculate Δn for the D_2 transition of an alkali-metal atom. The energy level scheme is shown in Fig. 2. Since the energy spacing between the two ground states is much larger than those of the excited states, the PS spectra for the transitions from the lower and upper hyperfine levels of the ground states are well separated. Thus, we consider the transitions from one of the two ground states, whose angular momentum quantum number is called F and the other is called F' (Fig. 2). As shown in Fig. 2, we measured the PS spectra with four transition schemes for ^{87}Rb and ^{85}Rb atoms.

First we consider two specific energy levels $|F_g,m\rangle$ and $|F_e,m+q\rangle$ with $q=\pm 1$. Since the real part of the complex refractive index (n_q) has the Kramers-Kronig relation $n_q=1-(\delta/k\Gamma)\alpha_q$ with the absorption coefficient α_q [2], the refractive index for the transition between $|F_g,m\rangle$ and $|F_e,m+q\rangle$ is given by

$$n_q = 1 - \frac{3\lambda^3}{4\pi^2} N \frac{\Delta/\Gamma}{1+4\Delta^2/\Gamma^2} R_{F_g,m}^{F_e,m+q}(P_{F_g}^m - Q_{F_e}^{m+q}), \tag{4}$$

where Δ is the frequency detuning of the probe beam relative to the resonance line between two energy levels under consideration, Γ is the decay rate of the excited state, N is the atomic density, λ is the wavelength corresponding to the atomic resonance, $q=\pm 1$ for $\sigma^{\pm}$ transition, and $P_{F_g}^{m_g}$ $(Q_{F_e}^{m_e})$ denotes the population at the ground (excited) state $|F_g,m_g\rangle$ $(|F_e,m_e\rangle)$. In Eq. (4), the normalized line strength is given by [16]

$$R_{F_g,m_g}^{F_e,m_e} = (2L_e+1)(2J_e+1)(2J_g+1)(2F_e+1)(2F_g+1) \times \left[\begin{Bmatrix} L_e & J_e & S \\ J_g & L_g & 1 \end{Bmatrix} \begin{Bmatrix} J_e & F_e & I \\ F_g & J_g & 1 \end{Bmatrix} \times \begin{pmatrix} F_g & 1 & F_e \\ m_g & m_e-m_g & -m_e \end{pmatrix} \right]^2,$$

where L, S, and I denote the orbital, electron spin, and nuclear spin angular momenta, respectively, and the curly (round) brackets represents the $6J$ $(3J)$ symbol.

To calculate the refractive index difference $(\Delta n=n_+-n_-)$ for the D_2 transition of an alkali-metal atom, it is necessary to sum up all the contributions from each transition. In the rest frame of an atom moving with a velocity v, the atom feels the pump and the probe beams with the detunings given by $\delta_{pu}=\delta+kv$ and $\delta_{pr}=\delta-kv$, respectively, where $\delta=\omega-(E_{F_e=F_g+1}-E_{F_g})/\hbar$ is the laser detuning with a laser angular frequency of ω and E_{F_e} (E_{F_g}) is the energy of the excited (ground) state. The change of the refractive index difference should be averaged over the Maxwell-Boltzmann velocity distribution

$$\Delta n(\delta,t) = -\frac{3\lambda^3}{4\pi^2}\frac{N}{\sqrt{\pi}u}\int_{-\infty}^{\infty} dv e^{-(v/u)^2} \times \sum_{F_e=F_g-1}^{F_g+1} \frac{(\delta_{pr}+\Delta_{F_e}^{F_g+1})/\Gamma}{1+4(\delta_{pr}+\Delta_{F_e}^{F_g+1})^2/\Gamma^2} \times \sum_{m=-F_g}^{F_g} \sum_{q=\pm 1} R_{F_g,m}^{F_e,m+q} q[P_{F_g}^m(t) - Q_{F_e}^{m+q}(t)], \tag{5}$$

where $\hbar\Delta_{F_e}^{F_e'}=E_{F_e'}-E_{F_e}$ is the hyperfine energy spacing of the

excited states and the most probable velocity is $u=(2k_BT/m)^{1/2}$.

Next, we calculate all the populations in Eq. (5) for given δ and v. We have performed similar calculations such as those in Ref. [15]. Since the details of the calculations are presented elsewhere [17], we provide a brief description of the calculation here. We consider a circular laser beam of radius a with a uniform intensity. Then the fraction of atoms that traverse the laser beam within t and $t+dt$ is given by

$$H(t)dt=\frac{1}{t}\left(-1+\frac{\sqrt{\pi}}{2\eta}(1+2\eta^2)e^{-\eta^2}\mathrm{erfi}(\eta)\right)dt,$$

where $\eta=2a/(ut)$ and $\mathrm{erfi}(x)=\mathrm{erf}(ix)/i$ is the imaginary error function [15]. Thus the averaged refractive index difference is given by

$$\Delta n(\delta)=\int_0^\infty \Delta n(\delta,t)H(t)dt, \tag{6}$$

where $\Delta n(\delta,t)$ is given in Eq. (5).

In calculating Eq. (6), we need to know the populations of all relevant levels at all times. To facilitate the calculation, we define the following functions:

$$A_{F_g}^m(t)=H(t)P_{F_g}^m(t),\quad B_{F_e}^m(t)=H(t)Q_{F_e}^m(t),$$

$$U_{F_g}^m(t)=\int_0^t A_{F_g}^m(t')dt',\quad V_{F_g}^m(t)=\int_0^t B_{F_g}^m(t')dt'.$$

Then, the refractive index difference averaged over time is given by

$$\begin{aligned}\Delta n(\delta)=&-\frac{3\lambda^4}{8\pi^{7/2}u}\sum_{F_e=F_g-1}^{F_g+1}\int_{-\infty}^{\infty}d\delta_{\mathrm{pu}}\\&\times\exp\left[-\left(\frac{\delta_{\mathrm{pu}}-\delta}{ku}\right)^2\right]\frac{(2\delta-\delta_{\mathrm{pu}}+\Delta_{F_e^g}^{F_g+1})/\Gamma}{1+4(2\delta-\delta_{\mathrm{pu}}+\Delta_{F_e^g}^{F_g+1})^2/\Gamma^2}\\&\times\sum_{m=-F_g}^{F_g}\{R_{F_g,m}^{F_e,m+1}[U_{F_g}^m(\infty)-V_{F_e}^{m+1}(\infty)]\\&-R_{F_g,m}^{F_e,m-1}[U_{F_g}^m(\infty)-V_{F_e}^{m-1}(\infty)]\}.\end{aligned} \tag{7}$$

In Eq. (7), we have changed the integration variable from v to $\delta_{\mathrm{pu}}=\delta+kv$. This is because we can calculate the populations and population-related functions as functions of only δ_{pu} from the rate equations. Equation (7) is the final result, which provides the PS spectra including resonance and crossover lines, and the remaining task is to calculate the values $U_{F_g}^m(\infty)$ and $V_{F_e}^m(\infty)$ from the rate equations as functions of δ_{pu}. The explicit expressions for the rate equations are displayed in the Appendix.

III. EXPERIMENTS

In order to verify the developed theory, we performed an experiment on the PS for the D_2 transitions of rubidium atoms. The layout of the experimental setup is shown in Fig. 1. An anamorphic prism pair and two lenses were used to collimate a beam with a spot radius of 2 mm. Both of the probe and pump beams were derived from an external cavity diode laser (ECDL) (Toptica, DL100) with a linewidth of <1 MHz. Two polarizing beam splitters (PBSs) were set up as in Fig. 1 to make the probe beam have pure polarization. The angle $\theta(\simeq 45°)$ of the probe beam's plane of polarization was adjusted by a $\lambda/2$ plate to make $I_x=I_y$ in the absence of the pump beam. Thus, as mentioned in Sec. II, all effects other than rubidium vapor such as two glass windows can be compensated. A $\lambda/4$ plate was used to make the pump beam have a circular polarization. The crossing angle between the probe and the counterpropagating pump beam in the vapor cell was about 10 mrad. The Rb cell was kept at room temperature and enclosed by a μ-metal magnetic shield to eliminate all of the outside magnetic field. For such a dilute Rb cell, the collisional broadening can be neglected [18]. The power of the pump and the probe beams was independently varied by neutral density filters. The two output signals from the PBS were focused onto photodiodes that were connected to a circuit to linearly convert the current to voltage. The voltage signals were electrically subtracted to yield the PS spectra. The intensity of the probe beam was 0.29 $\mu\mathrm{W/mm^2}$, whereas that of the pump beam was varied.

IV. RESULTS AND DISCUSSION

Figure 3 shows experimental and theoretical results where the intensity of the pump beam is $s_0(=I_{\mathrm{pu}}/I_s)=0.2$ (with $I_s=1.62$ $\mathrm{mW/cm^2}$ the saturation intensity). The thick (thin) curves of the upper traces in Figs. 3(a)–3(d) represent the experimental (calculated) PS spectra for the transition $F_g=1\rightarrow F_e=0,1,2$ of ^{87}Rb, $F_g=2\rightarrow F_e=1,2,3$ of ^{87}Rb, $F_g=2\rightarrow F_e=1,2,3$ of ^{85}Rb, and $F_g=3\rightarrow F_e=2,3,4$ of ^{85}Rb, corresponding to schemes (i), (ii), (iii), and (iv) in Fig. 2, respectively. In the bottom of each figure of Fig. 3, saturated absorption spectra are shown to facilitate identification of the position of signals. Here, the polarization of the pump beam is σ^+ and that of the probe beam is σ^+ or σ^-. In Fig. 3, L_μ denotes the resonance line for the transition $F_g\rightarrow F_e=\mu$ and $X_{\mu\nu}$ represents the crossover lines between the transitions $F_g\rightarrow F_e=\mu$ and $F_g\rightarrow F_e=\nu$.

By comparing the theoretical and the experimental traces, we easily see that our model reproduces accurately experimental features in the hyperfine transitions spectra. In particular, the PS spectra for the transitions from the lower hyperfine levels [Figs. 3(a) and 3(c)], which have not been expected based on other theories, are in good agreement with the calculated results. In the case of the upper hyperfine transitions [Figs. 3(b) and 3(d)], the largest anisotropies are generated for the closed transitions ($2\rightarrow 3$ for ^{87}Rb and $3\rightarrow 4$ for ^{85}Rb). These dispersion signals have the large amplitudes and steep slopes that can be used in laser frequency stabilization. As can be expected in Eq. (7), all the resonance and crossover lines are composed of several dispersive functions. The complicated line shapes in Fig. 3 resulted from the summation of several dispersive functions with various amplitudes and linewidths. This phenomenon was confirmed by our recent work on analytic calculation of the line shapes of the PS spectra [19].

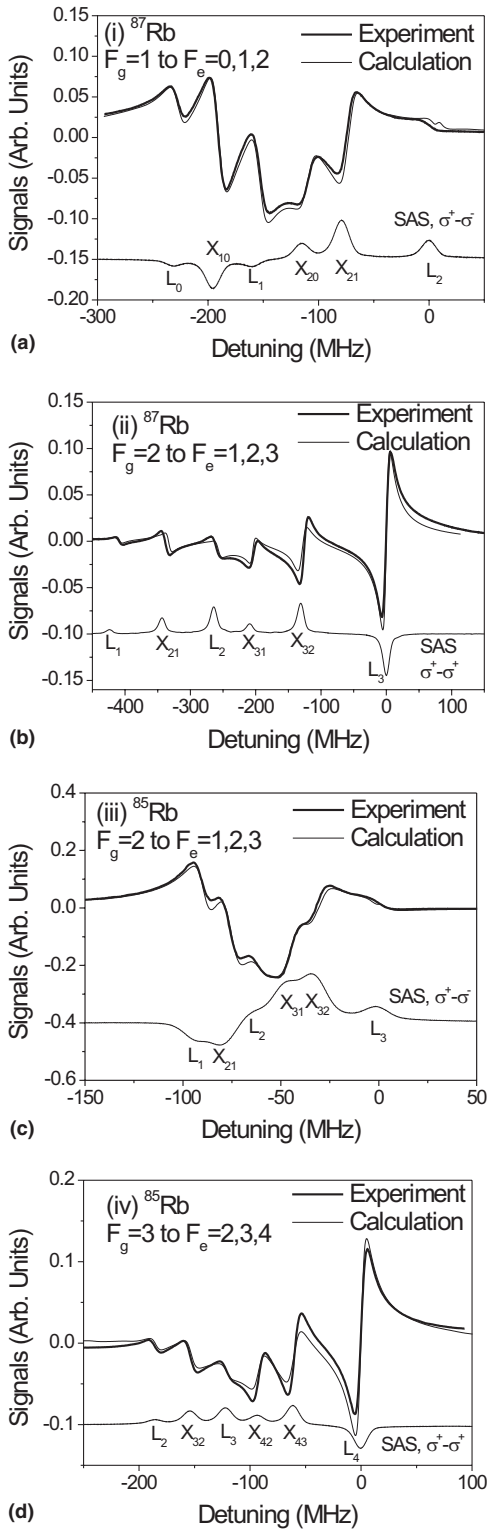

FIG. 3. The experimental and calculated PS spectra for transition from the lower hyperfine level of ^{87}Rb (a), the upper hyperfine level of ^{87}Rb (b), the lower hyperfine level of ^{85}Rb (c), and the upper hyperfine level of ^{85}Rb (d).

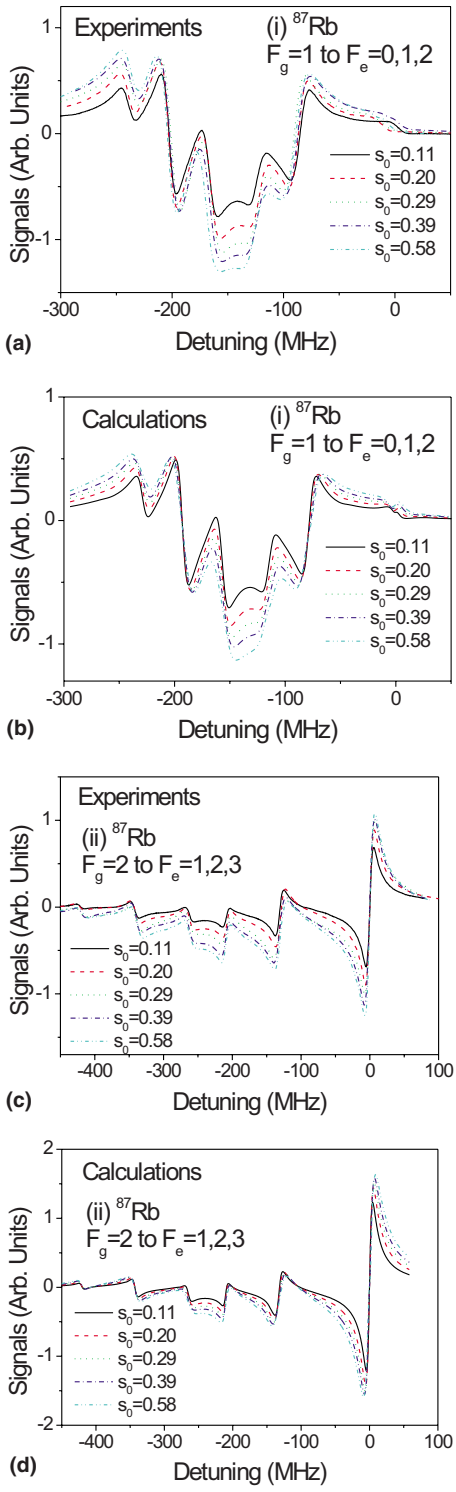

FIG. 4. (Color online) The experimental (a) and calculated (b) intensity dependence of the PS spectra for the transition $F_g=1\rightarrow F_e=0,1,2$ of ^{87}Rb atoms: The experimental and calculated results for the transition $F_g=2\rightarrow F_e=1,2,3$ of ^{87}Rb atoms are presented in (c) and (d), respectively.

In order to further verify our model, we varied the intensity of the pump beam. Figures 4(a) and 4(b) [Figs. 4(c) and 4(d)] show the experimental and calculated results for the lower [upper] hyperfine transition of ^{87}Rb, respectively, corresponding to scheme (i) [(ii)] in Fig. 2. The intensities of the pump beams were $s_0=0.11$, 0.20, 0.29, 0.39, and 0.58. In Fig. 4, we can see good agreement between the experimental and calculated results for all pump beam intensities. As the

intensity increased, we observed that the signals became broad, which we ascribed to the power broadening. In the case of the upper hyperfine transitions [Figs. 4(c) and 4(d)], as the intensity increased, the magnitude of the dispersive signal increased, while the slope remained almost unchanged. As can be seen in Fig. 4, the model, based on rate-equation approximation, worked very well for the intensities used in this experiment.

V. CONCLUSIONS

In this paper, we presented a description of our theoretical and experimental study on the polarization spectra for rubidium atoms. Our model for multilevel atoms provides an effective and computationally tractable method for calculating the polarization spectra. The populations of all the magnetic sublevels were calculated from the rate equations and used in calculating the PS spectra. The resulted PS spectra were then averaged over various transit times of the atom crossing the pump laser beam. We performed the calculation for the entire detuning range of the spectra and therefore could obtain the results that were in good agreement with experimental spectral features including the resonance and crossover lines. We could account for all of the PS spectra obtained for both rubidium isotopes with great accuracy. The theoretical model, developed in this paper, is generally applicable to other atoms such as Na or Cs. We are currently working on calculations and experiments for other transitions or other atoms.

ACKNOWLEDGMENTS

This work was supported by the Ministry of Commerce, Industry and Energy of Korea through the Industrial Technology Infrastructure Building Program.

APPENDIX

The rate equations for the ground state under consideration ($F_g=F$), the other ground state ($F_g=F'$), and the excited states are given by

$$\frac{d}{dt}P_F^m = -\sum_{F_e=F-1}^{F+1} R_{F,m}^{F_e,m+q'} \frac{\Gamma s_0}{2} \frac{P_F^m - Q_{F_e}^{m+q'}}{1+4(\delta_{\rm pu}+\Delta_{F_e}^{F+1})^2/\Gamma^2} + \sum_{F_e=F-1}^{F+1} \sum_{m_e=m-1}^{m+1} \Gamma R_{F,m}^{F_e,m_e} Q_{F_e}^{m_e}, \tag{A1}$$

$$\frac{d}{dt}P_{F'}^m = \sum_{F_e=F'-1}^{F'+1} \sum_{m_e=m-1}^{m+1} \Gamma R_{F',m}^{F_e,m_e} Q_{F_e}^{m_e}, \tag{A2}$$

$$\frac{d}{dt}Q_{F_e}^m = R_{F,m-q'}^{F_e,m} \frac{\Gamma s_0}{2} \frac{P_F^{m-q'} - Q_{F_e}^m}{1+4(\delta_{\rm pu}+\Delta_{F_e}^{F+1})^2/\Gamma^2} - \sum_{F_g=F,F'} \sum_{m_g=m-1}^{m+1} \Gamma R_{F_g,m_g}^{F_e,m} Q_{F_e}^m, \tag{A3}$$

where q' represents the polarization of the pump beam and $s_0=I_{\rm pu}/I_s$ with $I_{\rm pu}$ the intensity of the pump beam and $I_s=1.62\ \mathrm{mW/cm^2}$ the saturation intensity. The value m runs from $-F_g$ to F_g or $-F_e$ to F_e for the populations of the ground states or the excited states, respectively, and $F_e=F+1,F,F-1$ in Eq. (A3).

The corresponding rate equations for A and B are given by

$$\frac{d}{dt}A_F^m = -\sum_{F_e=F-1}^{F+1} R_{F,m}^{F_e,m+q'} \frac{\Gamma s_0}{2} \frac{A_F^m - B_{F_e}^{m+q'}}{1+4(\delta_{\rm pu}+\Delta_{F_e}^{F+1})^2/\Gamma^2} + \sum_{F_e=F-1}^{F+1} \sum_{m_e=m-1}^{m+1} \Gamma R_{F,m}^{F_e,m_e} B_{F_e}^{m_e} + \frac{dH}{dt}P_F^m, \tag{A4}$$

$$\frac{d}{dt}A_{F'}^m = \frac{dH}{dt}P_{F'}^m + \sum_{F_e=F'-1}^{F'+1} \sum_{m_e=m-1}^{m+1} \Gamma R_{F',m}^{F_e,m_e} B_{F_e}^{m_e}, \tag{A5}$$

$$\frac{d}{dt}B_{F_e}^m = R_{F,m-q'}^{F_e,m} \frac{\Gamma s_0}{2} \frac{A_F^{m-q'} - B_{F_e}^m}{1+4(\delta_{\rm pu}+\Delta_{F_e}^{F+1})^2/\Gamma^2} - \sum_{F_g=F,F'} \sum_{m_g=m-1}^{m+1} \Gamma R_{F_g,m_g}^{F_e,m} B_{F_e}^m + \frac{dH}{dt}Q_{F_e}^m, \tag{A6}$$

$$\frac{d}{dt}U_{F_g}^m = A_{F_g}^m, \tag{A7}$$

$$\frac{d}{dt}V_{F_e}^m = B_{F_e}^m. \tag{A8}$$

In the rate equations of Eqs. (A1)–(A8), two arbitrary equations have to be replaced by the following equations representing the normalization condition:

$$\sum_{F_g,m_g} P_{F_g}^{m_g} + \sum_{F_e,m_e} Q_{F_e}^{m_e} = 1, \tag{A9}$$

$$\sum_{F_g,m_g} A_{F_g}^{m_g} + \sum_{F_e,m_e} B_{F_e}^{m_e} = H(t). \tag{A10}$$

[1] C. Wieman and T. W. Hänsch, Phys. Rev. Lett. **36**, 1170 (1976).
[2] W. Demtröder, *Laser Spectroscopy* (Springer, Berlin, 1998).
[3] J. B. Kim, H. J. Kong, and S. S. Lee, Appl. Phys. Lett. **52**, 417 (1988).
[4] G. P. T. Lancaster, R. S. Conroy, M. A. Clifford, J. Arlt, and K. Dholakia, Opt. Commun. **170**, 79 (1999).
[5] C. P. Pearman, C. S. Adams, S. G. Cox, P. F. Griffin, D. A. Smith, and I. G. Hughes, J. Phys. B **35**, 5141 (2002).
[6] Y. Yoshikawa, T. Umeki, T. Mukae, Y. Torii, and T. Kuga, Appl. Opt. **42**, 6645 (2003).
[7] A. Ratnapala, C. J. Vale, A. G. White, M. D. Harvey, N. R. Heckenberg, and H. Rubinsztein-Dunlop, Opt. Lett. **29**, 2704 (2004).
[8] V. B. Tiwari, S. Singh, S. R. Mishra, H. S. Rawat, and S. C. Mehendale, Opt. Commun. **263**, 249 (2006).
[9] A. C. Eckbreth, *Laser Diagnostics for Combustion Temperature and Species* (Gordon and Breach, Amsterdam, 1996).
[10] K. Danzmann, K. Grützmacher, and B. Wende, Phys. Rev. Lett. **57**, 2151 (1986).
[11] K. B. MacAdam, A. Steinbach, and C. E. Wieman, Am. J. Phys. **60**, 1098 (1992).
[12] D. A. Smith and I. G. Hughes, Am. J. Phys. **72**, 631 (2004).
[13] S. Nakayama, Jpn. J. Appl. Phys., Part 1 **24**, 1 (1985).
[14] S. Nakayama, Phys. Scr. **T70**, 64 (1997).
[15] M. L. Harris, C. S. Adams, S. L. Cornish, I. C. McLeod, E. Tarleton, and I. G. Hughes, Phys. Rev. A **73**, 062509 (2006).
[16] A. R. Edmonds, *Angular Momentum in Quantum Mechanics* (Princeton University Press, Princeton, 1960).
[17] G. Moon and H. R. Noh, J. Korean Phys. Soc. **50**, 1037 (2007).
[18] O. Schmidt, K. M. Knaak, R. Wynands, and D. Meschede, Appl. Phys. B: Lasers Opt. **59**, 167 (1994).
[19] H. D. Do, M. S. Heo, G. Moon, H. R. Noh, and W. Jhe (unpublished).